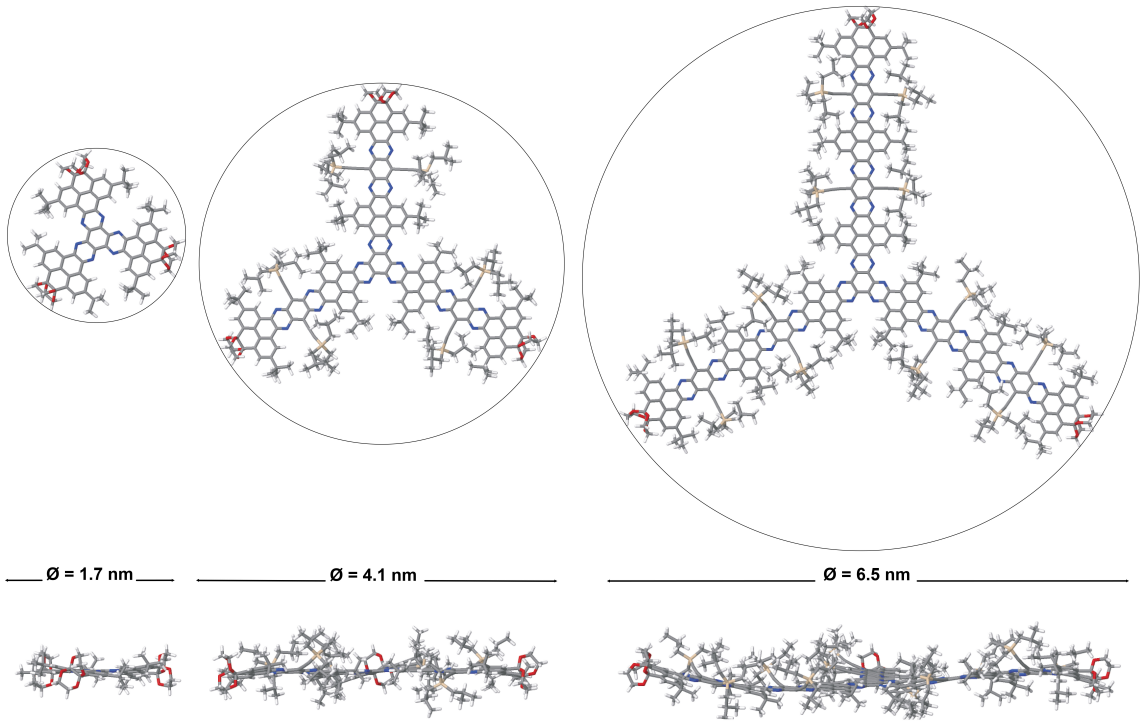

Figure S1. SNG-G_0 (left), **SNG-G_1** (middle) and **SNG-G_2** (right) computed with GFN-xTB.

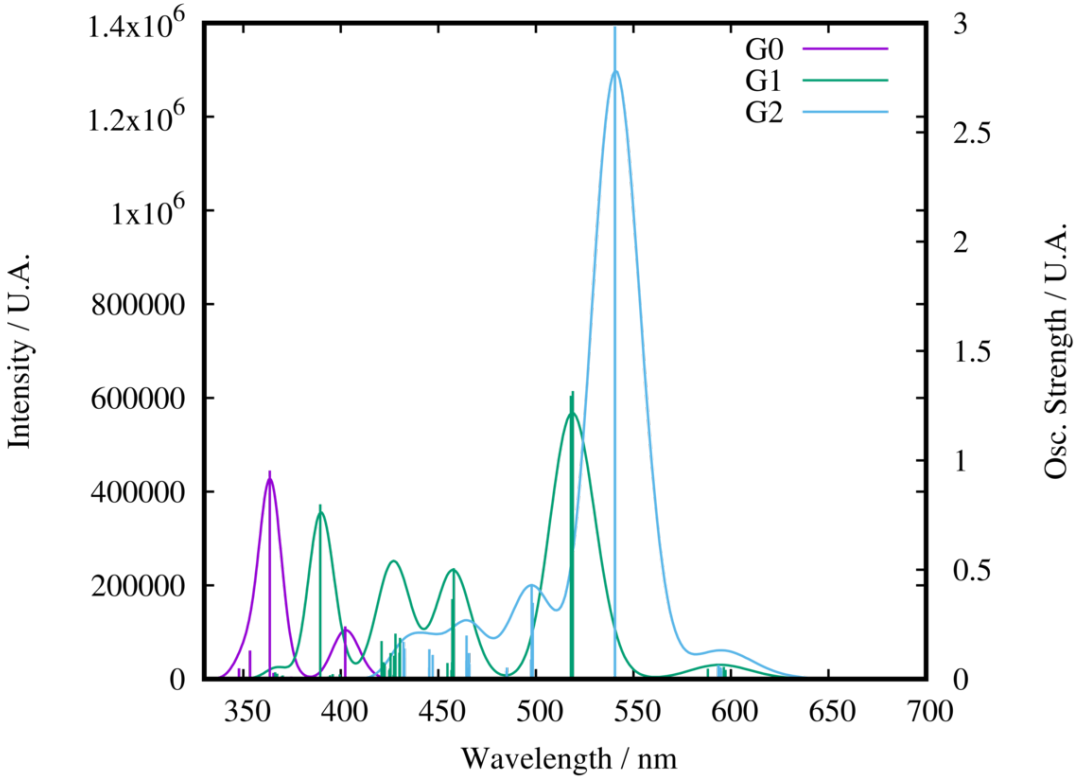

Figure S2. Absorption spectra for **SNG-G_0-H**, **SNG-G_1-H** and **SNG-G_2-H** at the B3LYP-6-31g(d) level in vacuum (96 excitations), the simulated spectra (intensity vs. wavelength) is represented by a continuous line, while the oscillator strength of each transition is represented by sticks.

	Trans.	eV	nm	Osc. Strength	Major contribs
SNG-G_0-H	1	3.1	402	0.24	HOMO->LUMO (93%)
SNG-G_0-H	11	3.4	364	0.95	H-1->L+1(44%), HOMO->L+2 (44%)
SNG-G_1-H	1	2.1	597	0.04	HOMO->LUMO (96%)
SNG-G_1-H	10	2.4	519	1.32	H-3->L+1 (41%), H-4->LUMO(16%), H-4->L+1(21%)
SNG-G_2-H	1	2.0	613	0.01	HOMO->L+1 (96%)
SNG-G_2-H	28	2.3	541	2.98	H-6->L+1(27%),H-6->L+2 (26%), H-7->L+1(18%)

Table S1. TD-DFT first and strongest transitions at the B3LYP-6-31g(d) level for **SNG-G_0-H**, **SNG-G_1-H**, and **SNG-G_2-H**. All values in eV.

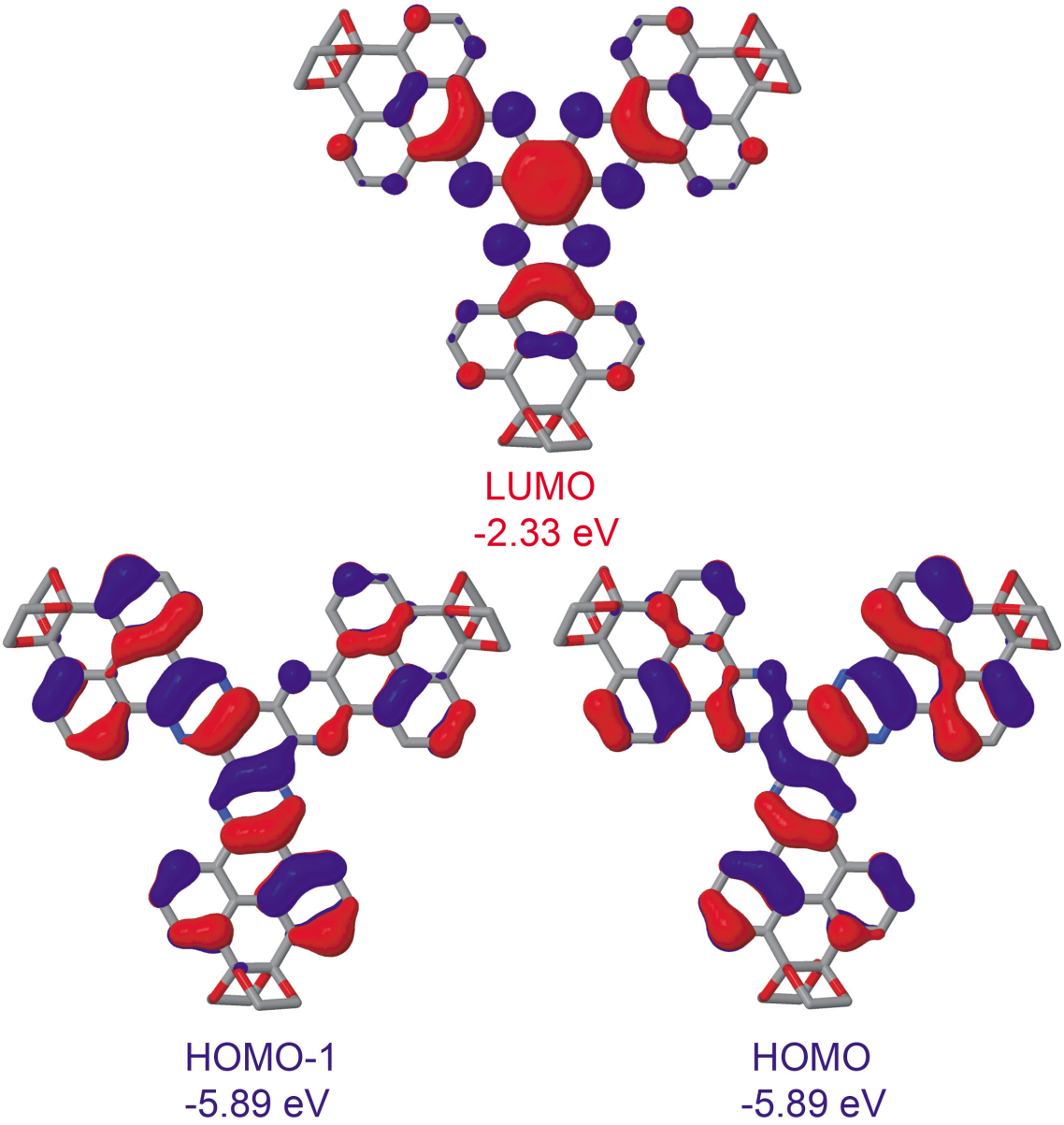

Figure S3. B3LYP-6-31g(d) level frontier orbitals for **SNG-G_0-H**.

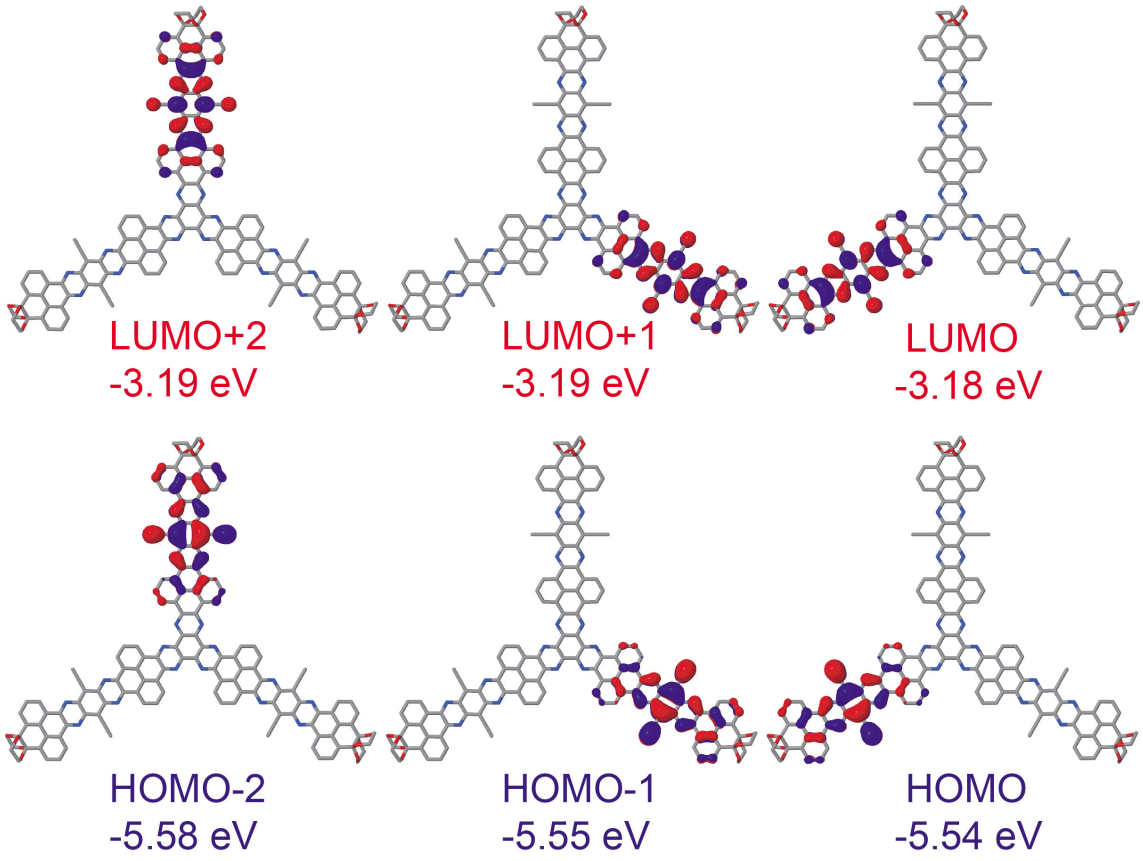

Figure S4. B3LYP-6-31g(d) level frontier orbitals for **SNG-G$_1$-H**.

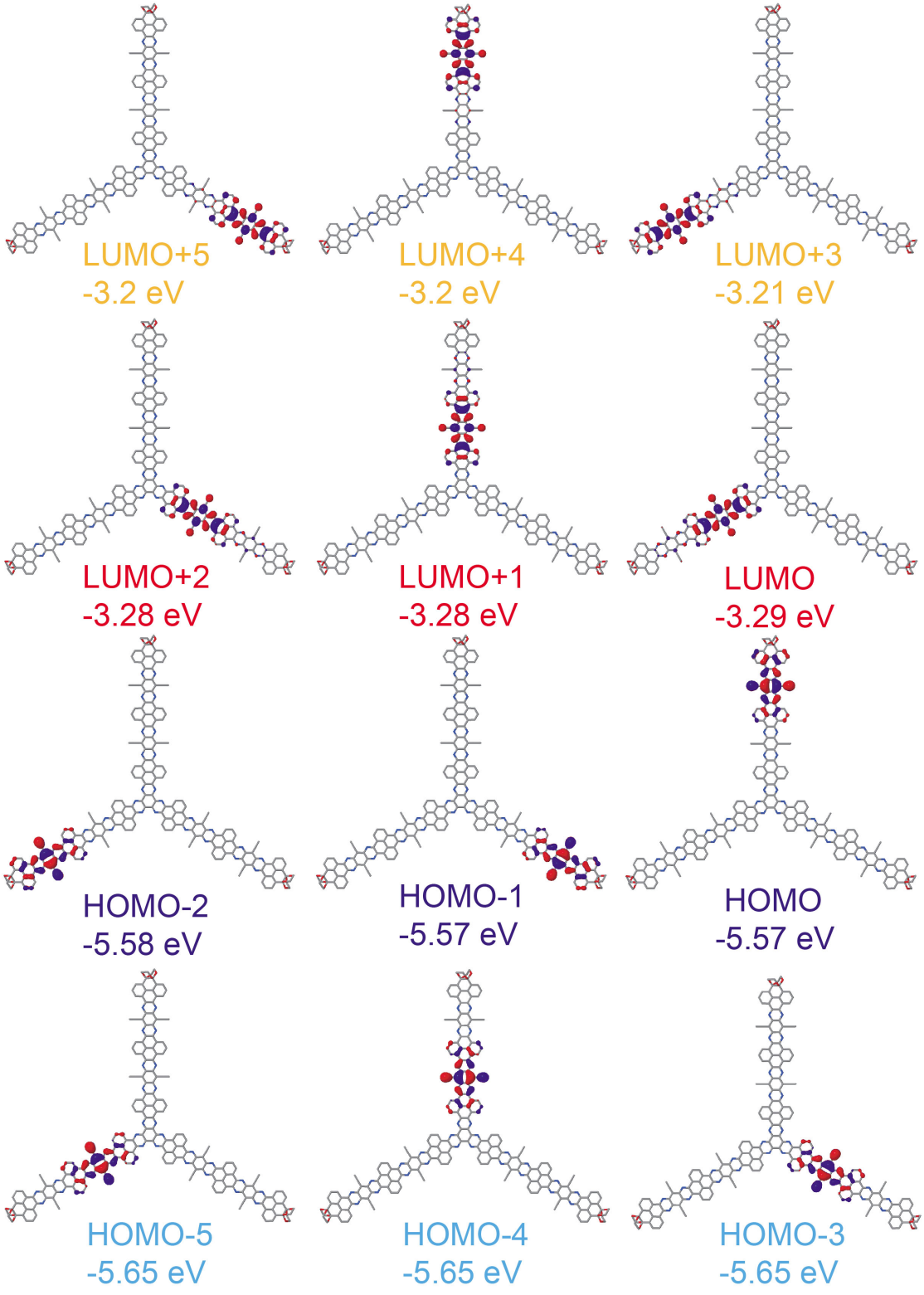

Figure S5. B3LYP-6-31g(d) level frontier orbitals for **SNG-G_2-H**.

B3LYP-6-31g(d)/GFN-xTB																		Gap
SNG-G_0	-0.76	-0.8	-0.8	-0.92	-0.92	-0.93	-2.06	-2.06	-2.24	-5.7	-5.71	-5.77	-5.9	-5.91	-6.28	-6.29	-6.37	3.46
SNG-G_1	-1.64	-1.66	-1.67	-2.31	-2.32	-2.47	-3.14	-3.16	-3.16	-5.33	-5.34	-5.34	-5.8	-5.8	-5.94	-5.97	-5.98	2.17
SNG-G_2	-2.35	-2.36	-2.51	-3.17	-3.19	-3.2	-3.22	-3.23	-3.28	-5.36	-5.37	-5.38	-5.4	-5.42	-5.44	-5.82	-5.83	2.08
B3LYP-6-31g(d)/GFN-xTB																		
SNG-G_0-H	-0.86	-0.89	-0.89	-1.03	-1.04	-1.04	-2.16	-2.16	-2.35	-5.88	-5.88	-6.09	-6.16	-6.16	-6.38	-6.39	-6.39	3.53
SNG-G_1-H	-1.71	-1.72	-1.72	-2.4	-2.4	-2.57	-3.2	-3.21	-3.21	-5.53	-5.54	-5.54	-5.9	-5.9	-6.13	-6.23	-6.24	2.32
SNG-G_2-H	-2.46	-2.47	-2.61	-3.2	-3.2	-3.21	-3.28	-3.28	-3.29	-5.57	-5.57	-5.58	-5.65	-5.65	-5.65	-5.94	-5.94	2.28
B3LYP-6-31g(d)																		
SNG-G_0-H	-0.9	-0.93	-0.93	-1.08	-1.09	-1.09	-2.17	-2.17	-2.33	-5.89	-5.89	-6.09	-6.17	-6.17	-6.47	-6.49	-6.49	3.56
SNG-G_1-H	-1.71	-1.71	-1.71	-2.4	-2.42	-2.55	-3.18	-3.19	-3.19	-5.54	-5.55	-5.58	-5.91	-5.92	-6.14	-6.21	-6.22	2.35
SNG-G_2-H	-2.46	-2.47	-2.61	-3.2	-3.2	-3.21	-3.28	-3.28	-3.29	-5.57	-5.57	-5.58	-5.65	-5.65	-5.65	-5.94	-5.94	2.28
B3LYP-6-311+g(2d,g)/B3LYP-6-31g(d)																		
SNG-G_0-H	-1.26	-1.32	-1.32	-1.48	-1.48	-1.49	-2.48	-2.48	-2.74	-6.15	-6.15	-6.39	-6.46	-6.46	-6.79	-6.84	-6.85	3.41
SNG-G_1-H	-2.07	-2.08	-2.08	-2.72	-2.74	-2.97	-3.54	-3.55	-3.56	-5.86	-5.87	-5.89	-6.18	-6.19	-6.42	-6.52	-6.54	2.3
SNG-G_2-H	-2.79	-2.79	-3.03	-3.58	-3.58	-3.58	-3.65	-3.65	-3.65	-5.9	-5.9	-5.9	-5.97	-5.97	-5.97	-6.22	-6.22	2.25

Table S2. Frontier orbitals were computed with the B3LYP Hamiltonian with the 6-31g(d) basis set in vacuum for all geometries and the 6-311+g(2d,p) basis set for the SNG-G_x-H geometries. SNG-G_x molecules were optimised only at the GFN-xTB level while SNG-G_x-H geometries were optimised at the GFN-xTB and the B3LYP-6-31g(d) levels. The colour code is LUMOs, HOMOs and gaps. All values in eV.

(B3LYP-6-31g(d)/GFN-xTB) - (B3LYP-6-31g(d))																		Gap
SNG-G_0-H	-0.04	-0.04	-0.04	-0.05	-0.05	-0.05	-0.01	-0.01	0.02	-0.01	-0.01	0	-0.01	-0.01	-0.09	-0.1	-0.1	0.03
SNG-G_1-H	0	0.01	0.01	0	-0.02	0.02	0.02	0.02	0.02	-0.01	-0.01	-0.04	-0.01	-0.02	-0.01	0.02	0.02	0.03
SNG-G_2-H	0	0	0	0	0	0	0	0	0	0	0	0	0	0	0	0	0	0

Table S3. Frontier orbitals eigenvalues B3LYP-6-31g(d) differences for SNG-G_x-H geometries optimised a the GFN-xTB and the B3LYP-6-31g(d) level. The colour code is LUMOs, HOMOs and gaps. All values in eV.

				$\phi\Sigma\mu$_Max [10^{-9} m^2 V^{-1} s^{-1}]			$\Delta\sigma$_Max [10^{-9} S cm^{-1}]		Half-lifetime [10^{-7} s]		
	WL [nm]	Power [10^{-2} W]	F [10^{5} m^{-3}]	Decay	Manual	Average	Decay	Manual	half	peak	half-peak
SNG-G_0	355	1.00	2.57	13.9	13.7	10.5	10.3	10.1	6.70	0.78	5.92
	355	1.00	2.57	7.84	7.30		5.79	5.39	4.64	1.58	3.06
SNG-G_1	355	1.00	2.57	10.0	9.83	9.8	7.39	7.26	5.90	0.90	5.00
	355	1.00	2.57	9.80	9.70		7.24	7.16	9.28	1.29	7.99
SNG-G_2	355	1.00	2.57	14.2	14.1	11.1	10.5	10.4	6.26	1.01	5.25
	355	1.00	2.57	8.12	8.07		6.00	5.96	6.01	1.25	4.76

Table S4. TRMC of **SNG-G_0**, **SNG-G_1** and **SNG-G_2** (λ = 355 nm, I_0= 9.1 x 10^{15} photons/cm^2).

Experimental Procedures

Synthesis and characterisation

Commercial chemicals and solvents were used as received. Analytical thin layer chromatography (TLC) was carried out using aluminum sheets (20x20 cm) pre-coated with silica gel RP-18W 60 F254 from Merck. Column chromatography was carried out using Silica gel 60 (40-60 μm) from Scharlab. NMR spectra in solution were recorded on a Bruker Avance 400 MHz or 500 MHz spectrometer at 298 K using partially deuterated solvents as internal standards. High Resolution Matrix Assisted Laser Desorption Ionization (coupled to a Time-Of-Flight analyzer) Mass Spectrometry experiments were recorded in Biomagune in a Ultraflex III (Bruker Daltonics) MALDI-ToF (frequency-tripled (355 nm) Nd:YAG laser) by Dr. Javier Calvo. Matrix Assisted Laser Desorption Ionization (coupled to a Time-Of-Flight analyzer) experiments MALDI-TOF) were recorded on Bruker REFLEX spectrometer in POLYMAT by Dr. Estíbaliz González de San Román Martín. Further evidence of the successful preparation of the SNGs came from MALDI-TOF HRMS that show ion peak masses $(M+Ag)^+$ of 1553.5692, 4211.1790, and 6868.7884 Da, respectively for **SNG-G$_0$**, **SNG-G$_1$** and **SNG-G$_2$**, that matched with the expected mass. The isotopic distributions could be only recorded for **SNG-G$_0$** and **SNG-G$_1$** due to the high molecular weight of **SNG-G$_2$**, which is at the detection limit of the technique that illustrates the extremely high molecular weight of these monodisperse systems.

Steady-state electronic absorption

Absorption spectra were recorded on a Perkin-Elmer Lambda 950 spectrometer.

Photoluminescence

Photoluminescence spectra were recorded on a LS55 Perkin-Elmer Fluorescence spectrometer.

Electrochemistry

Electrochemical measurements were carried out on a Princeton Applied Research Parstat 2273 in a 3-electrode single compartment cell with glassy carbon disc working electrode, a platinum wire counter electrode and a silver wire pseudoreference electrode. All the potential values are reported versus the redox potential of the ferrocene/ferrocenium couple.

Time-resolved microwave conductivity (TRMC)

A film on a quartz substrate was set in a resonant cavity and probed by continuous microwaves at ~9.1 GHz. The third harmonic generation (THG; 355 nm) of an Nd:YAG laser (Continuum Inc., Surelite II, 5-8 ns pulse duration, 10 Hz) was used as an excitation source (incident photon density, I0 = 9.1 × 1015 photons cm^{-2} $pulse^{-1}$). The photoconductivity transient Δσ was converted to the product of the quantum yield (φ) and the sum of the charge carrier mobilities, $\Sigma\mu = (\mu_h + \mu_e)$ by $\varphi\Sigma\mu = \Delta\sigma(eI_0F_{light})^{-1}$,

where e and F_{light} are the unit charge of a single electron and the correction (or filling) factor, respectively.

Synthesis of compound C.

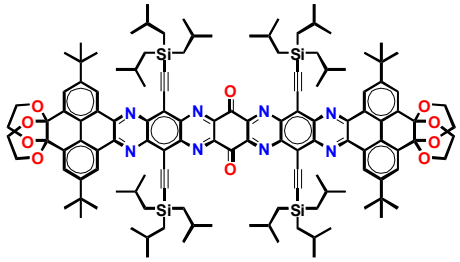

Compound **A** (45 mg, 0.045 mmol) and cyclohexane-1,2,3,4,5,6-hexaone (5 mg, 0.015 mmol) were dissolved in chloroform (9 mL) and acetic acid (3 mL) was added and the reaction was refluxed for 72 hours. Water was added and the product was extracted with chloroform (3 x 25 mL). The organic phase was dried over sodium sulfate, filtrated and removed by rotary evaporation. The crude was loaded onto a chromatographic column (eluent mixture chloroform:toluene 1:3). The solvent was removed under vacuum. Then, the resulting solid was dissolved in chloroform (3 mL) and MnO_2 (10 mg) was added to the solution was stirred for 1 hour. The brown solid was precipitated several times using a mixture of solvents dichloromethane and methanol, the product was obtained pure as bright brown solid (5 mg, 15 %).

^{1}H-NMR (400 MHz, $CDCl_3$): 9.53 (d, *J* = 2.1 Hz, 4H), 8.22 (d, 4H), 4.43 – 4.32 (br s, 8H), 3.91 – 3.75 (br s, 8H), 2.26 – 2.12 (m, 12H), 1.62 (s, 36H), 1.17 (d, *J* = 6.5 Hz, 72H); ^{13}C-NMR (100 MHz, $CDCl_3$): 177.59, 152.23, 146.29, 144.95, 143.56, 143.12, 132.72, 129.15, 127.57, 127.19, 125.21, 124.73, 116.95, 101.08, 93.28, 61.75, 35.53, 31.67, 26.59, 25.28, 25.06; MS (MALDI, pos.) (*m/z*): $[M+H]^+$ calcd. for $C_{130}H_{169}N_8O_{10}Si_4$: 2115.206, found: 2115.013.

Synthesis of SNG-G_0

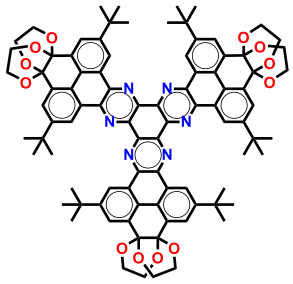

A solution of hexaaminobenzene (340 mg, 2.021 mmol) and 2,7-di-*tert*-butyl-10,11-dihydro-8b,12a-(epoxyethanooxy)pyreno[4,5-b][1,4]dioxine-4,5-dione (2.339 g, 5.056 mmol) in acetic acid (30 mL) was stirred at 100 °C under nitrogen for 16 h. The reaction was cooled down at room temperature and poured into water (50 mL) and stirred 30 minutes. The precipitate was filtrated and washed with water and methanol. The crude mixture was purified by chromatography column (silica gel dichloromethane/petroleum ether 7:3 and then dichloromethane 100 %) obtaining 1.33 g (45%) of a yellow solid.

^{1}H-NMR (400 MHz, $CDCl_3$): 9.90 (6H, *J* = 2.0 Hz, d), 8.33 (6H, *J* = 2.0 Hz, d), 4.43 (12H, *br* s), 3.91 (12H, *br* s), 1.73 (54H, s); ^{13}C-NMR (400 MHz, $CDCl_3$) 151.84, 143.36, 142.15, 132.43, 129.81, 126.89, 125.66, 124.27, 93.77, 61.99, 35.82, 32.30; MS (MALDI, pos.) (*m/z*): $[M+Ag]^+$ calcd. for $C_{90}H_{90}AgN_6O_{12}$: 1553.5668, found: 1553.5692.

Synthesis of SNG-G_0-Q

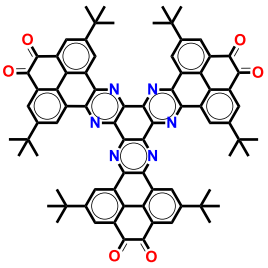

SNG-G_0 (124 mg, 0.086 mmol) was dissolved in a mixture of TFA/water (10 mL, 9:1) at 0 °C. The solution was stirred overnight at room temperature. The precipitate formed was filtrated and washed with water and hot methanol to get 70 mg (69%) of a yellow solid.

^{1}H-NMR (500 MHz, TFA-d_1): 10.62 (6H, J = 2.0, d), 9.48 (6H, J = 2.0 Hz, d), 2.28 (54H, s); ^{13}C-NMR (125 MHz, TFA-d_1): 183.89, 157.76, 145.61, 143.18, 135.78, 134.88, 132.63, 131.84, 131.21, 38.27, 33.03; MS (MALDI, pos.) (*m/z*): $[M+Ag]^+$ calcd. for $C_{78}H_{66}AgN_6O_6$: 1289.4095, found: 1289.4093.

Synthesis of SNG-G_1

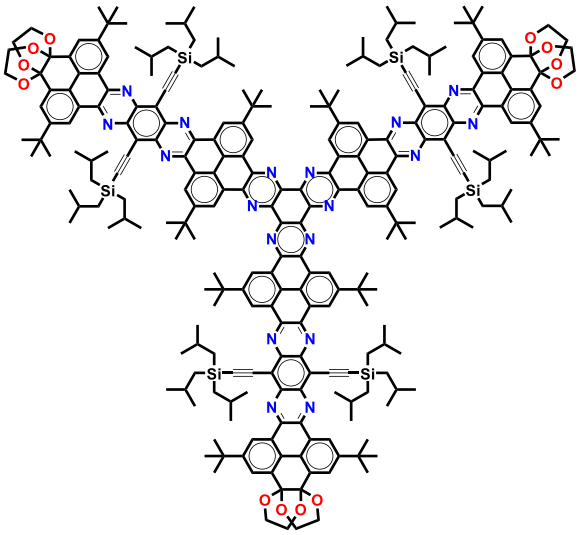

Compound **A** (106 mg, 0.105 mmol) and compound **SNG-G_0-Q** (25 mg, 0.021 mmol) were dissolved in chloroform (3 mL), acetic acid (1 mL) was added and the reaction was refluxed for 72 hours. Water was added and the product was extracted with chloroform (3 x 25 mL). The organic phase was dried over sodium sulfate, filtrated and removed by rotary evaporation. The crude was loaded onto a chromatographic column (eluent mixture chloroform:toluene 3:1). The resulting solid was precipitated in dichloromethane and methanol and the product was obtained as a bright red solid (27 mg, 32%).

^{1}H-NMR (400 MHz, $CDCl_3$): 10.46 (6H, s), 10.20 (6H, *J* = 2.0 Hz, s), 9.60 (6H, *J* = 2.0 Hz, s), 8.24 (6H, s), 4.49 – 4.32 (12H, *br* s), 3.98 – 3.79 (12H, *br s*), 2.27 – 2.11 (18H, m), 2.06 (54H, s), 1.67 (54H, s), 1.16 (144H, m); ^{13}C-NMR (100 MHz, $CDCl_3$): 151.86, 151.33, 144.78, 144.60, 143.70, 142.45, 142.21, 142.14, 132.43, 129.74, 129.61, 129.57, 127.13, 127.04, 126.74, 126.55, 126.31, 124.74, 121.90, 112.58, 102.52, 93.46, 61.76, 36.18, 35.56, 32.75, 31.80, 26.56, 25.31, 25.23; MS (MALDI, pos.) (*m/z*): $[M+Ag]^+$ calcd. for $C_{264}H_{318}AgN_{18}O_{12}Si_6$: 4211.2579, found: 4211.1790.

Synthesis of SNG-G_2

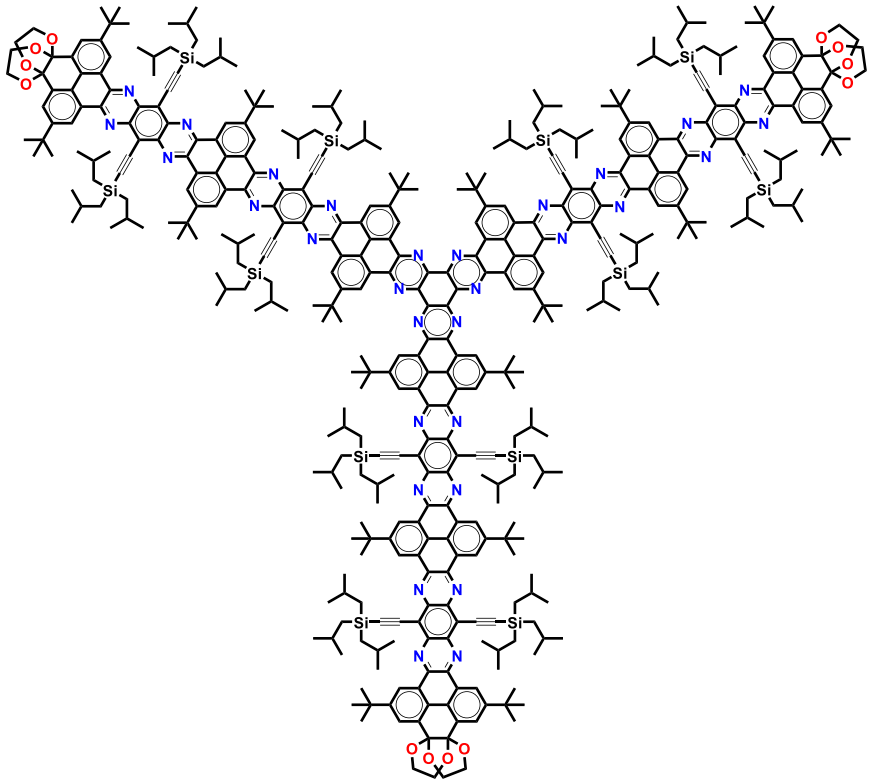

SNG-G_1 (10 mg, 2.43 µmol) was dissolved in TFA (3 mL) and water (1 mL) was added. The reaction was stirred at room temperature and followed by thin layer chromatography. Aqueous work-up was carried out and extracted with chloroform. The organic phase was dried over sodium sulfate anhydrous, filtrated and removed by rotary evaporation. The red solid was filtrated through a silica plug and used in the next step without further purification. The resulting red solid was dissolved in chloroform (3 mL) and acetic acid (1 mL) and compound **A** (14 mg, 14 µmol) was added. The reaction was refluxed for 72 hours. The crude was diluted with chloroform and washed with water (3 x 25 mL). The organic phase was dried over sodium sulfate anhydrous, filtrated and eliminated by rotary evaporation. The solid was loaded onto a chromatographic column (eluent mixture chloroform:toluene 4:1). The resulting solid was precipitated in dichloromethane and methanol. The product was obtained as a bright pink solid (6 mg, 38%).

^{1}H-NMR (500 MHz, $CDCl_3$): 10.55 – 10.43 (6H, m), 10.28 – 10.18 (6H, m), 10.13 – 9.91 (12H, m), 9.65 – 9.49 (6H, m), 8.29 – 8.16 (6H, m), 4.49 – 4.28 (12H, *br* s), 3.99 – 3.75 (12H, *br* s), 2.37 – 2.11 (36H, m), 2.09 (54H, s), 1.92 (54H, s), 1.66 (54H, s), 1.30 – 1.07 (m, 288H); ^{13}C-NMR (125 MHz, $CDCl_3$): 151.86, 151.35, 151.05, 144.92, 144.87, 144.63, 144.59, 143.74, 143.65, 142.50, 142.42, 142.37, 142.10, 132.41, 129.73, 129.69, 129.62, 127.37, 127.12, 126.82, 126.32, 125.44, 124.76, 122.00, 121.86, 121.80, 112.90, 112.81, 112.61, 112.55, 112.41, 102.50, 102.46, 102.39, 93.45, 61.79, 36.22, 35.99, 35.55, 32.78, 32.37, 31.80, 27.27, 26.60, 26.53, 25.37, 25.29, 25.17; MS (MALDI, pos.) (*m/z*): $[M+Ag]^+$ calcd. for $C_{438}H_{548}AgN_{30}O_{12}Si_{12}$: 6868.0154, found: 6868.7884.

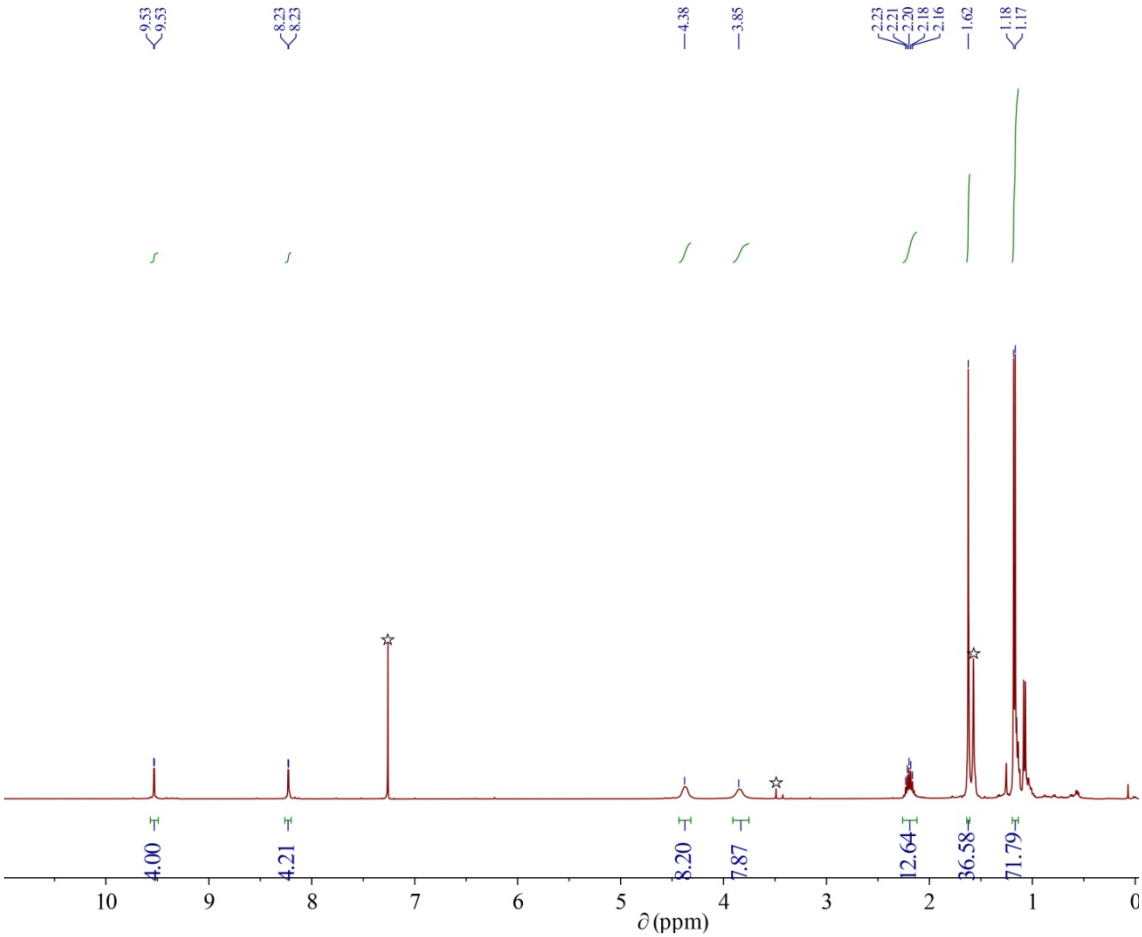

Figure S6. ^{1}H NMR of the compound **C** in $CDCl_3$.

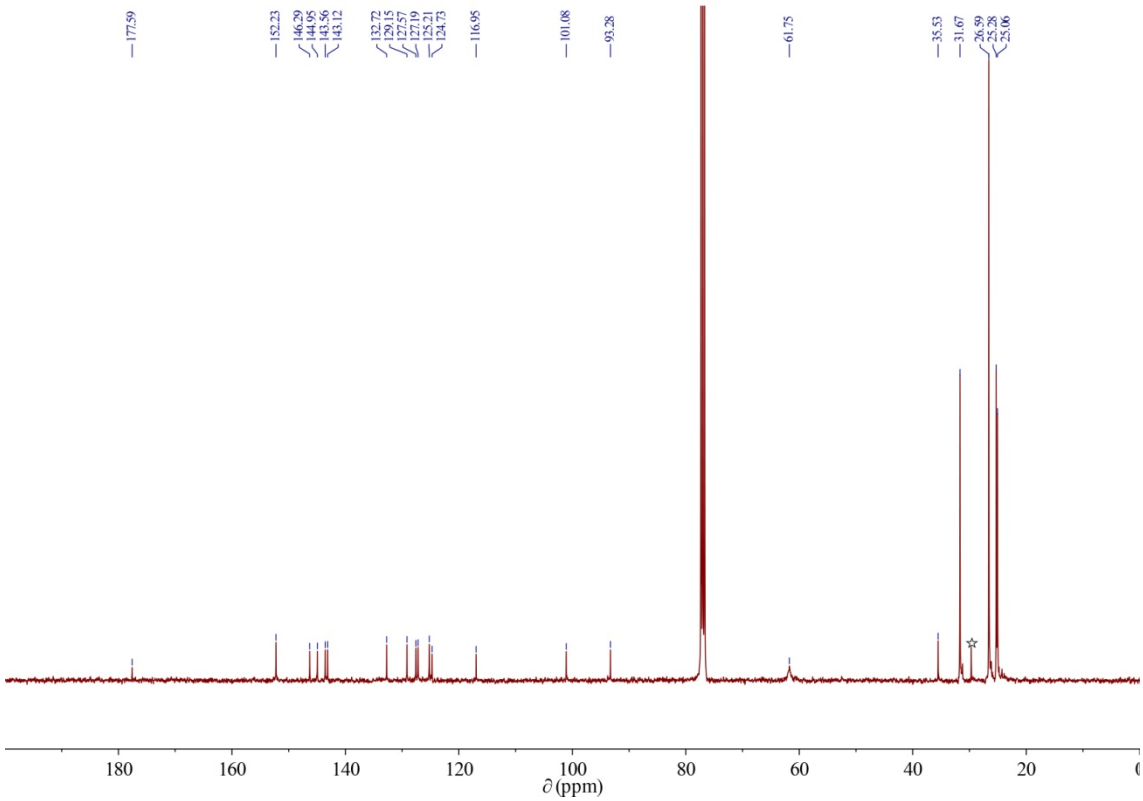

Figure S7. ^{13}C NMR of the compound **C** in $CDCl_3$.

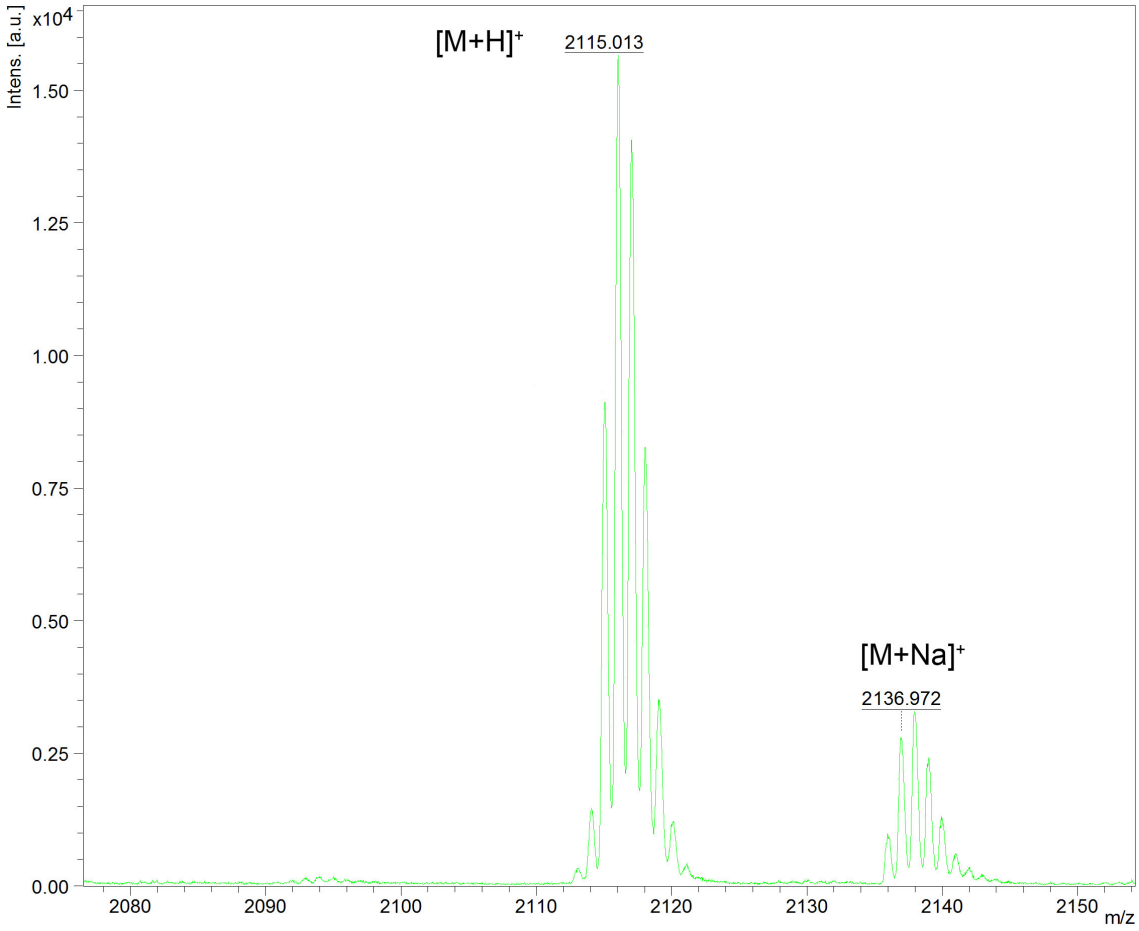

Figure S8. MALDI-TOF of the compound **C** .

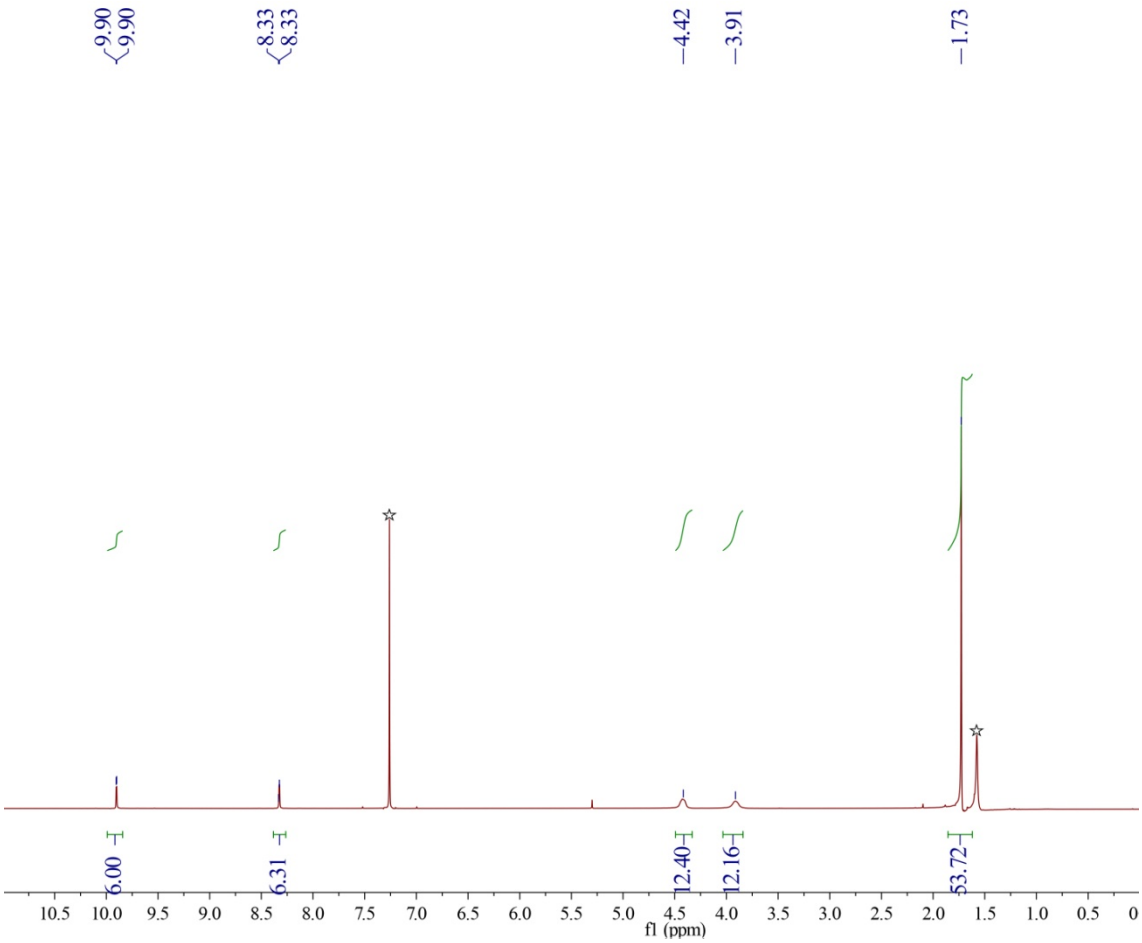

Figure S9. ^{1}H NMR of the compound **SNG-G$_0$** in $CDCl_3$.

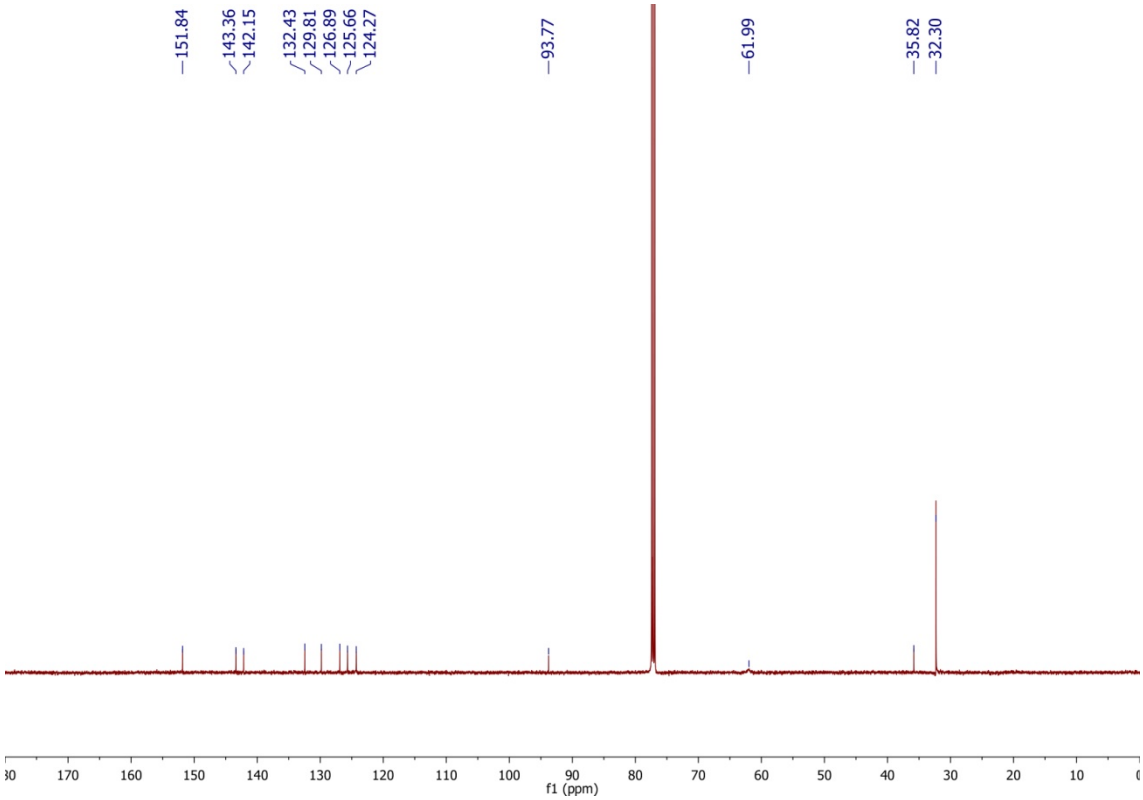

Figure S10. ^{13}C NMR of the compound **SNG-G$_0$** in $CDCl_3$.

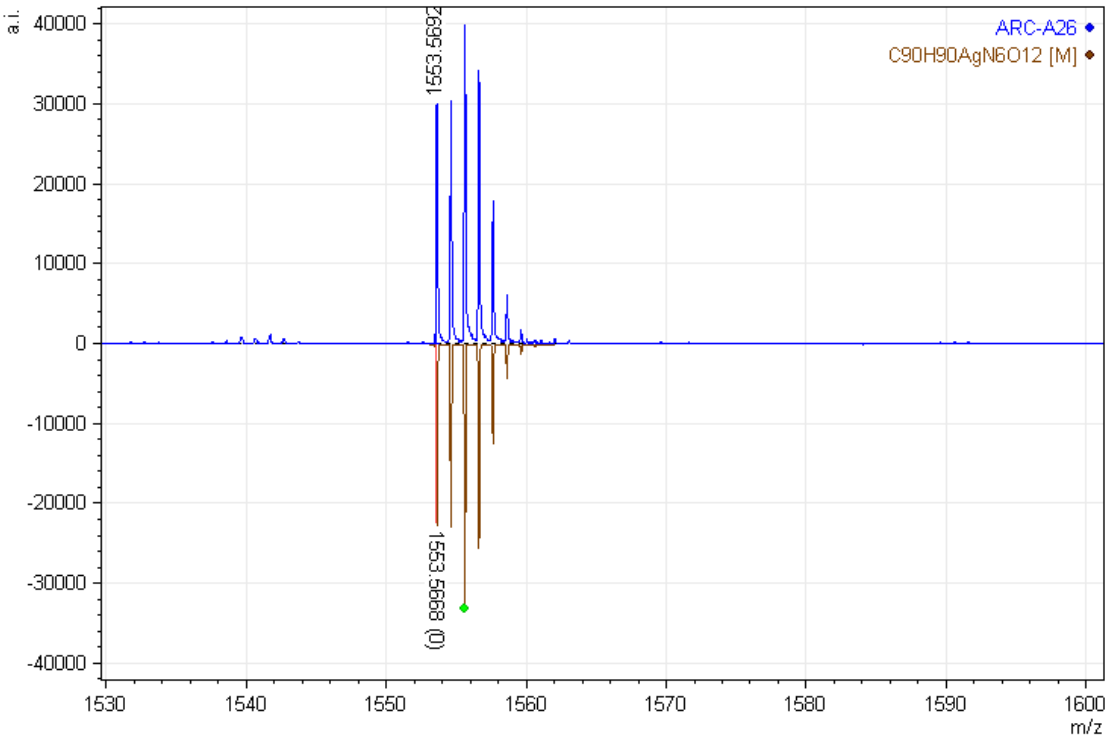

Figure S11. MALDI-TOF of the compound **SNG-G_0**.

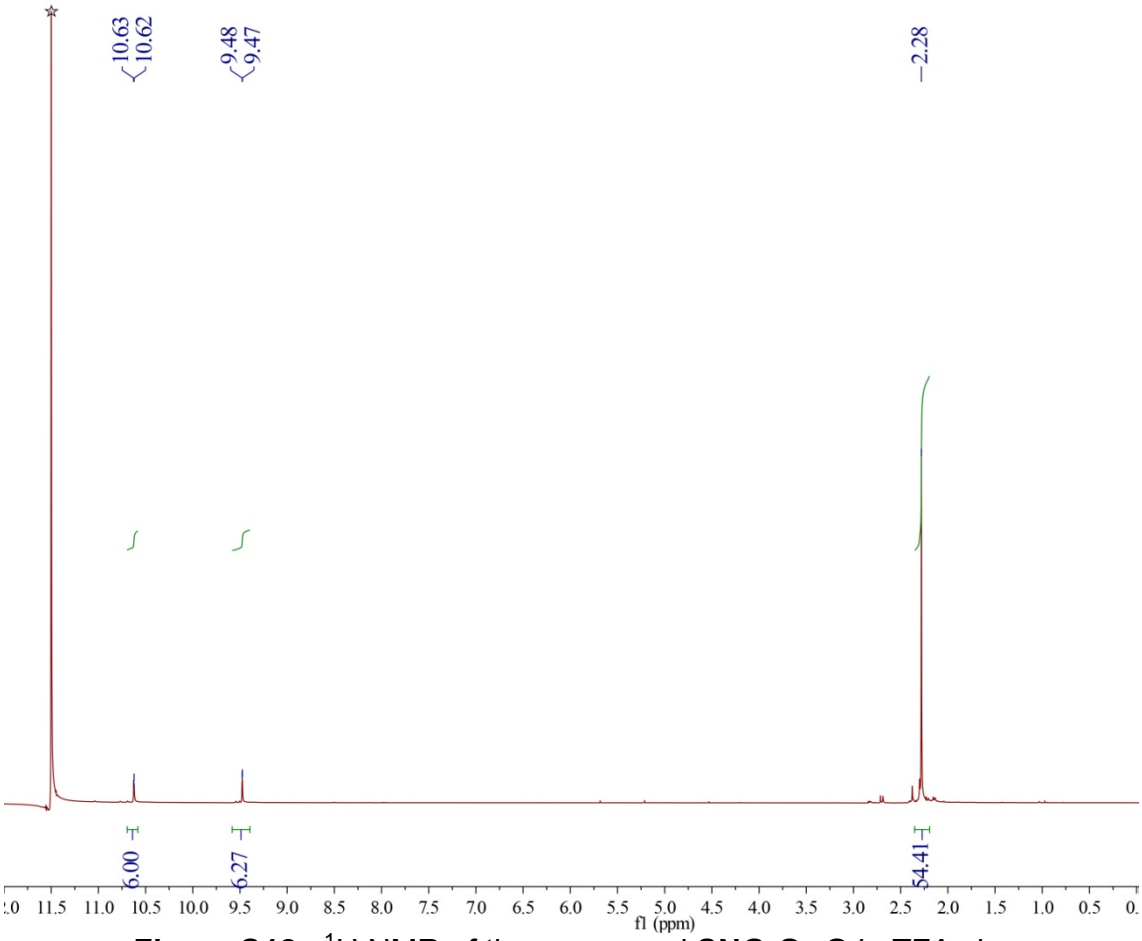

Figure S12. ^{1}H NMR of the compound **SNG-G$_0$-Q** in TFA-d_1.

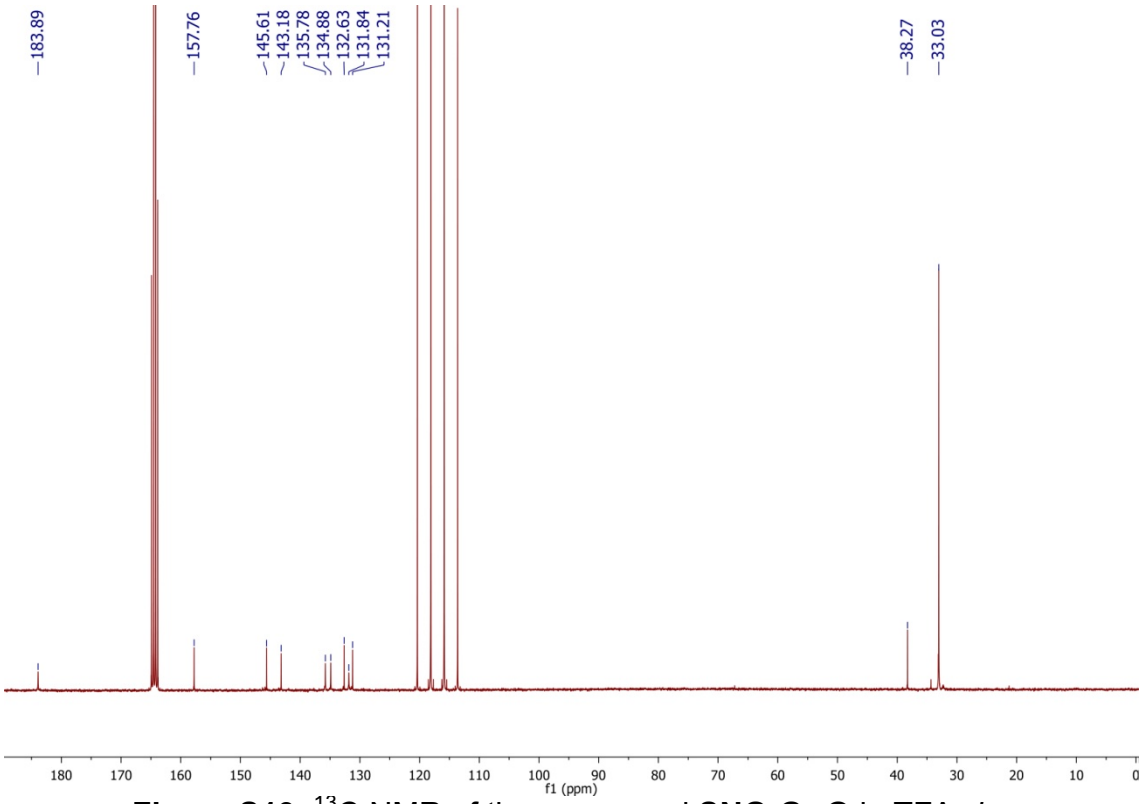

Figure S13. ^{13}C NMR of the compound **SNG-G$_0$-Q** in TFA-d_1.

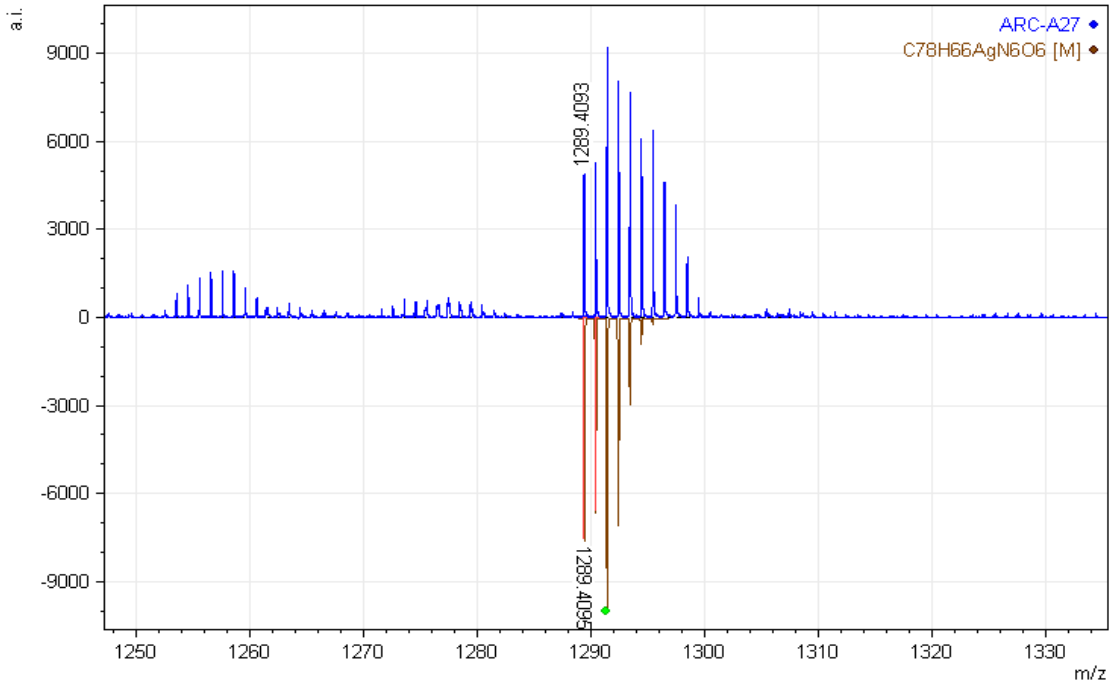

Figure S14. MALDI-TOF of the compound **SNG-G_0-Q.**

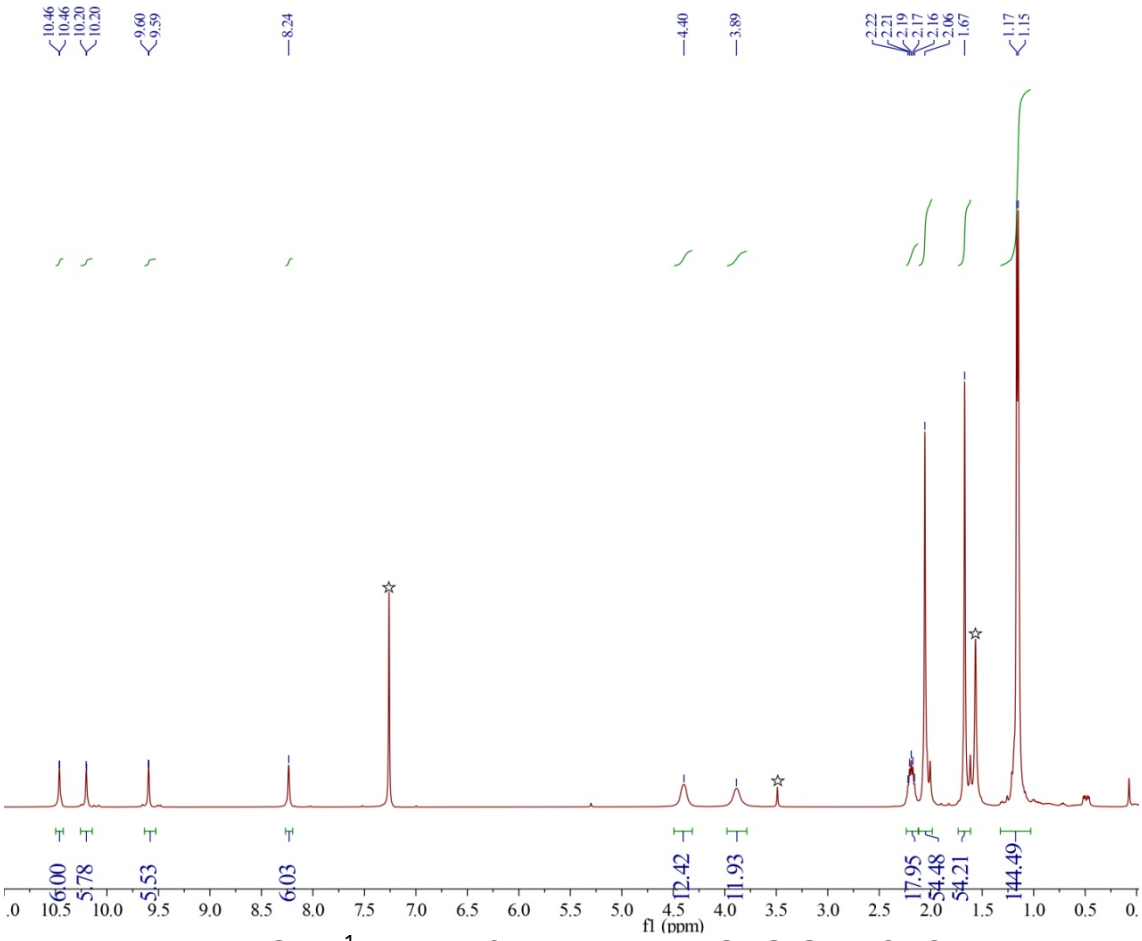

Figure S15. ^{1}H NMR of the compound **SNG-G$_1$** in $CDCl_3$.

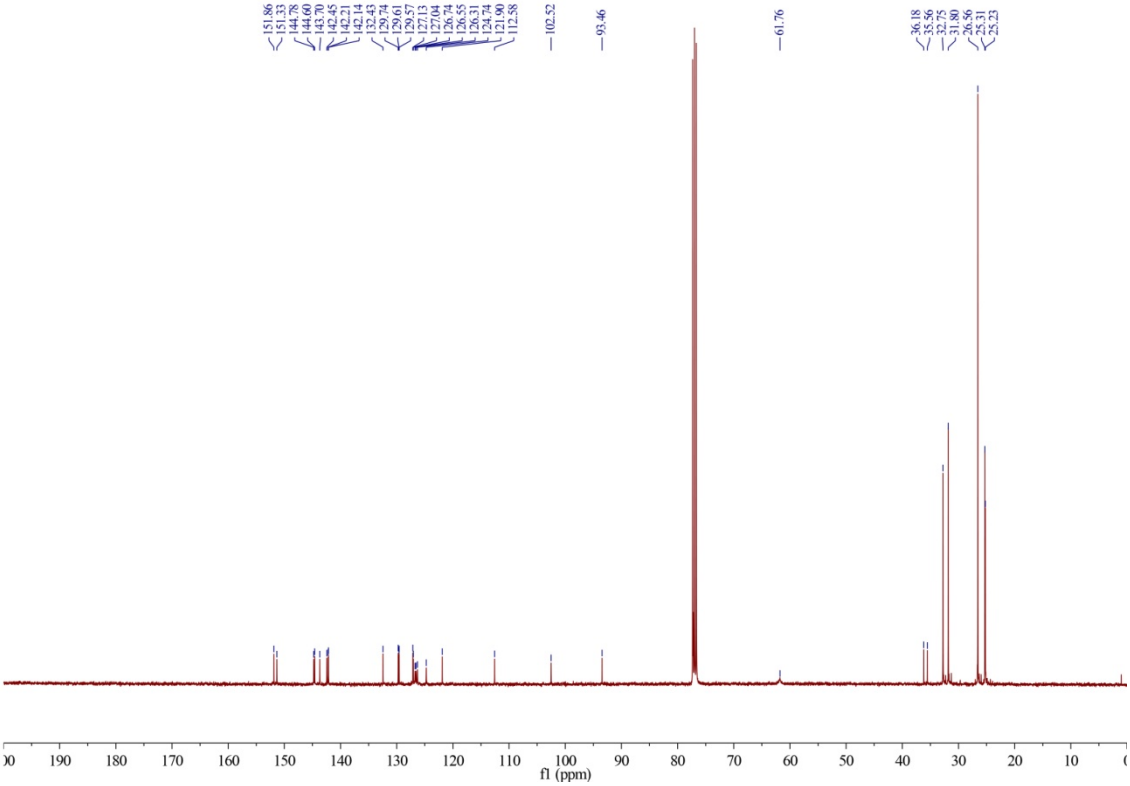

Figure S16. ^{13}C NMR the compound **SNG-G$_1$** in $CDCl_3$.

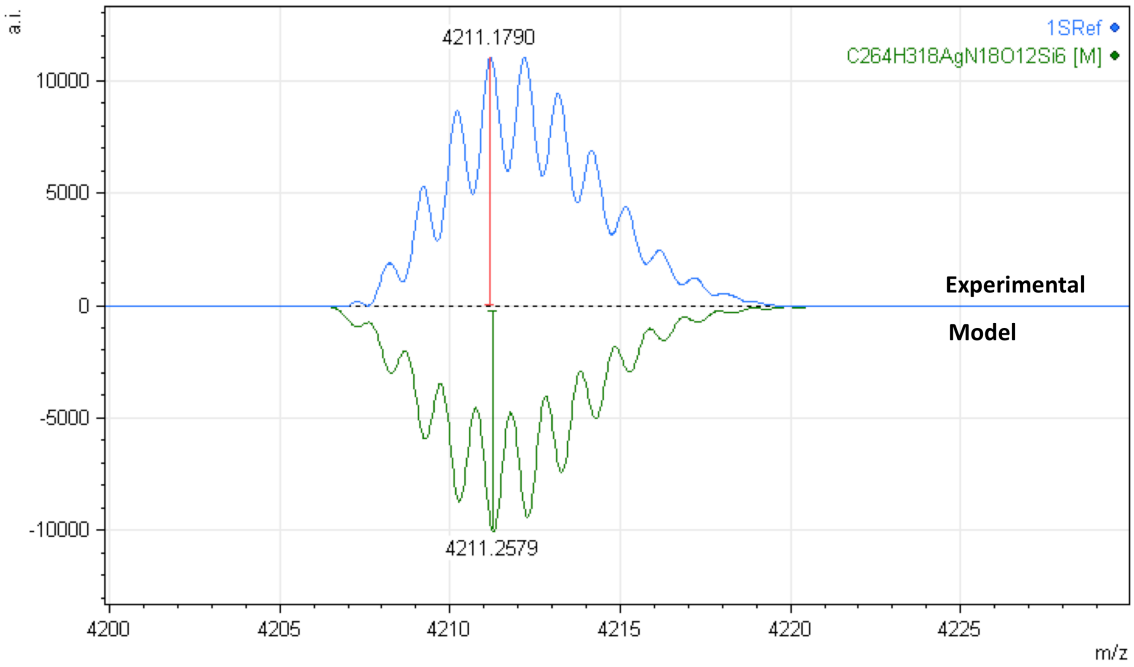

Figure S17. MALDI-TOF of the compound **SNG-G$_1$**.

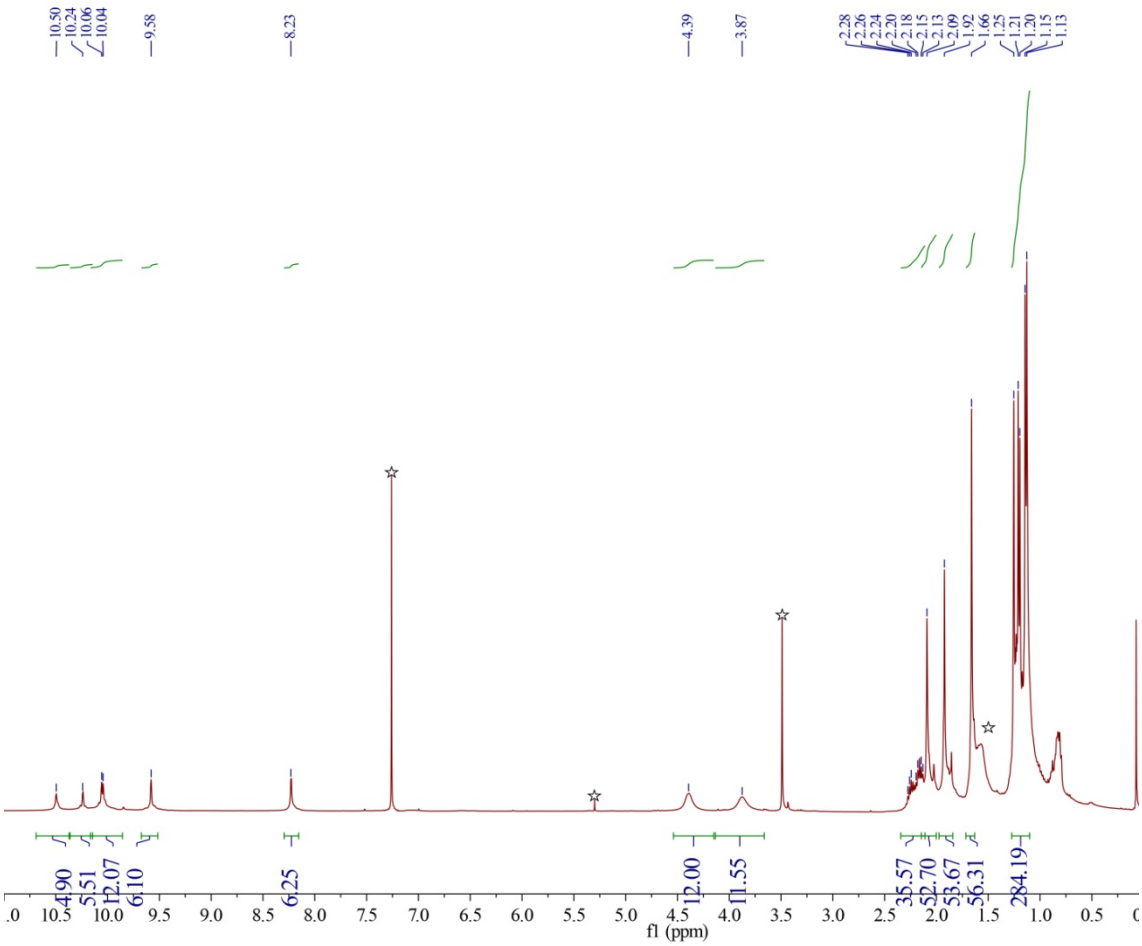

Figure S18. ^{1}H NMR of the compound **SNG-G$_2$** in $CDCl_3$.

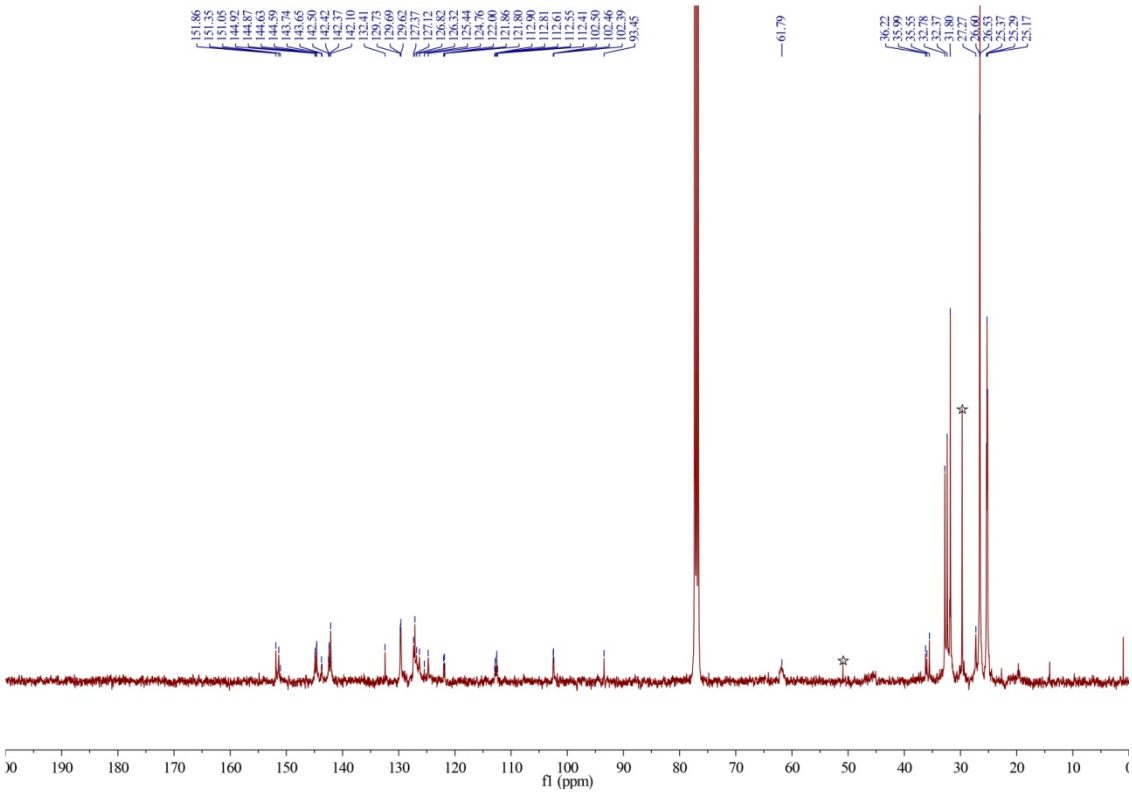

Figure S19. ^{13}C NMR the compound **SNG-G_2** in $CDCl_3$.

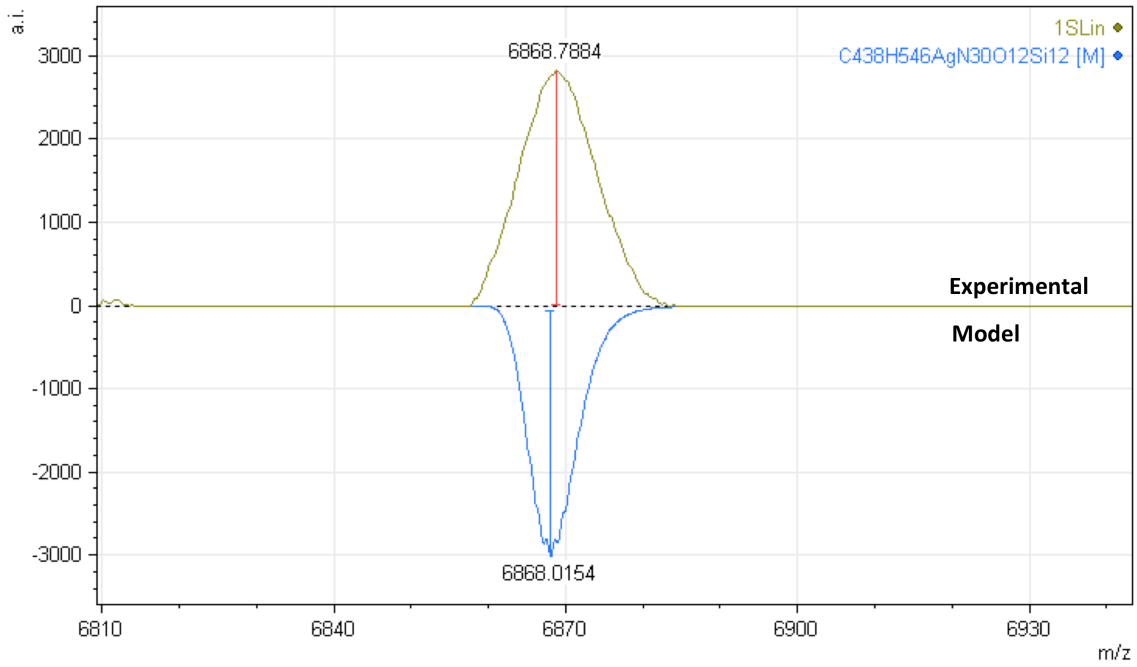

Figure S20. MALDI-TOF of the compound **SNG-G_2.**

References

[1] D. Cortizo-Lacalle, J. P. Mora-Fuentes, K. Strutyński, A. Saeki, M. Melle-Franco, A. Mateo-Alonso, *Angew. Chem. Int. Ed.* **2018**, *57*, 703-708.
[2] D. Z. Rogers, *J. Org. Chem.* **1986**, *51*, 3904-3905.